International Journal of Thermophysics, Vol. 12, No. 4, 1991

Interferometric Technique for the Subsecond Measurement of Thermal Expansion at High Temperatures: Applications to Refractory Metals[1]

A. P. Miiller[2] and A. Cezairliyan[2]

A high-speed interferometric technique has been developed at the National Institute of Standards and Technology to measure thermal expansion of metals between room temperature and temperatures primarily in the range 1500 K to near their melting points. The basic method involves resistively heating the specimen from room temperature up to and through the temperature range of interest in less than 1 s by passing an electrical current pulse through it and simultaneously measuring, with submillisecond resolution, the specimen temperature by means of a high-speed photoelectric pyrometer and the shift in the fringe pattern produced by a Michelson-type interferometer. The polarized beam from a He–Ne laser in the interferometer is split into two components, one which undergoes successive reflections from highly polished flats on opposite sides of the specimen and one which serves as the reference beam. The linear thermal expansion of the specimen is determined from the cumulative fringe shift corresponding to each measured temperature. The technique is capable of measuring linear thermal expansion with a maximum estimated uncertainty which ranges from about 1% at 2000 K to approximately 2% at 3600 K. Measurements have been performed on the refractory metals, niobium, molybdenum, tantalum, and tungsten, yielding thermal expansion data in the temperature range 1500 K up to near their respective melting points. Also, the technique has been used to follow the rapid dimensional changes that occur during solid–solid phase transformations; in particular, the $\alpha \rightarrow \gamma$ transformation in iron has been studied.

KEY WORDS: high temperature; interferometry; iron; molybdenum; niobium; pulse heating; solid-solid phase transformations; tantalum; thermal expansion; tungsten.

[1] Invited paper presented at the Tenth International Thermal Expansion Symposium, June 6–7, 1989, Boulder, Colorado, U.S.A.

[2] Thermophysics Division, National Institute of Standards and Technology, Gaithersburg, Maryland 20899, U.S.A.

0195-928X/91/0700-0643$06.50/0

1. INTRODUCTION

Measurements of thermal expansion at temperatures above about 1100 K generally rely on steady-state techniques such as push-rod dilatometry, X-ray diffractometry, or optical comparator methods. The long heating periods (minutes to hours) required by these techniques, however, tend to create problems associated with large heat transfers, loss of mechanical strength, evaporation, specimen contamination, etc., which become particularly severe at temperatures above 2000 K. In order to minimize such difficulties, we developed a high-speed interferometric technique [1] in which the entire experiment is performed in less than 1 s. This involved constructing a Michelson-type interferometer and adapting it to an existing pulse-heating system [2, 3] at the NIST (National Institute of Standards and Technology, formerly National Bureau of Standards).

Upon completion of its development, our high-speed interferometric technique was used to measure the thermal expansion of several refractory metals in succession, namely, tantalum [1], molybdenum [4], niobium [5], and tungsten [6], at temperatures in the range 1500 K up to near their respective melting points. The applicability of the technique for measuring rapid dimensional changes during solid–solid phase transformations was also established [7]. During the course of this work, several refinements and improvements were made in the construction and operation of the interferometric and data acquisition systems, as well as in the method of data analysis.

The objective of the present paper is twofold: (1) to describe briefly the salient features of the interferometric measurement system, including improvements that have been made, and (2) to summarize and correlate the results that were obtained from the earlier measurements.

2. MEASUREMENT METHOD

The method is based on rapid resistive self-heating of the specimen from room temperature to the maximum temperature of interest by the passage of a subsecond-duration electrical current pulse through it and on simultaneously measuring, with submillisecond resolution, the specimen temperature by means of a high-speed photoelectric pyrometer [8] and the shift in the fringe pattern produced by the interferometer. A functional diagram of the measurement system is given in Fig. 1. The polarized beam from a He–Ne laser in the interferometer is split into two component beams, one which undergoes successive reflections from highly polished flats on opposite sides of the specimen and one which serves as the reference beam. The linear thermal expansion of the specimen is determined

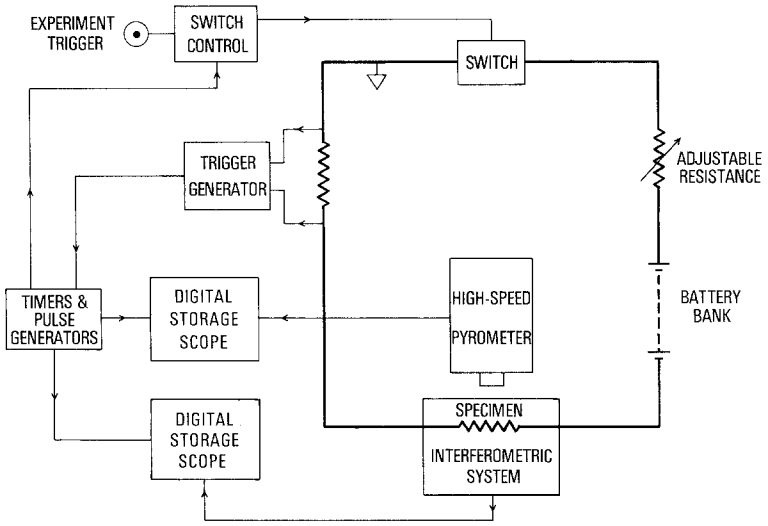

Fig. 1. Functional diagram of the thermal expansion measurement system.

from the cumulative fringe shift corresponding to each measured specimen temperature.

The discussion related to instrumentation in this paper deals only with the salient features of the interferometric system. Detailed descriptions concerning the construction and operation of the interferometric system [1], the pulse-heating system [2, 3] and the high-speed pyrometer [8] are given in the cited publications.

3. INTERFEROMETRIC SYSTEM

As shown in Fig. 2, the interferometric system consists of a polarized Michelson-type interferometer, in which the specimen acts as a double retroreflector, and a phase-quadrature detector.

The specimen (shown in cross section) is a long precision-machined tube with two parallel highly polished flats on opposite sides along its length. The nominal dimensions are as follows: length, 76 mm; inside diameter, 5.3 mm; outside diameter, 6.6 mm; distance between parallel flats, 6.1 mm. The latter dimension is the so-called specimen "length," l_0, in the expansion measurements. A small rectangular sighting hole (0.5×1 mm) in the wall at the middle of the tube provides an approximation to blackbody conditions for optical temperature measurements.

A polarizing beam-splitter (PB1) separates the beam from a linearly

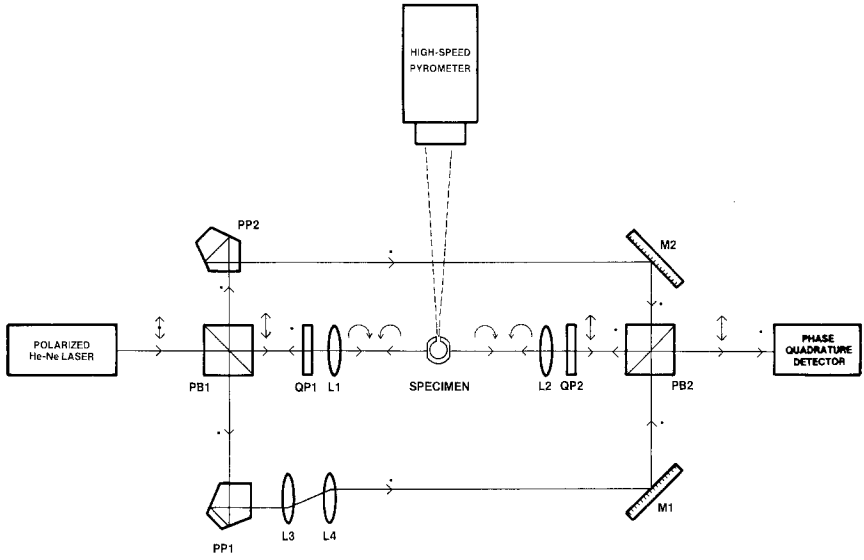

Fig. 2. Schematic diagram of the interferometer consisting of the following optical elements: polarizing beamsplitters PB1 and PB2; quarter-wave plates QP1 and QP2; lenses L1, L2, L3, and L4; pentaprisms PP1 and PP2; and plane mirrors M1 and M2. Polarization states of the beams are indicated by double-headed arrows (p-polarization), heavy dots (s-polarization, and curved arrows (circular polarization).

polarized He–Ne laser into two component beams. One component (s-polarized) is reflected around the specimen into the detector by optical elements PP1, L3, L4, M1, and PB2 and, thus, serves as the reference beam. The other component (p-polarized) is first directed through quarter-wave plate QP1 (oriented at 45°), to convert its polarization from linear to circular, and is then focused by lens L1 onto the "front" surface of the specimen. Upon retroreflection, the sense of circular polarization is reversed so that, after a second pass through QP1, the beam is again linearly polarized, but now with s-polarization. This enables the beam to be reflected around the specimen by PB1, PP2, and M2. By a similar consideration of optical elements PB2, QP2, and L2, one can show that, after retroreflection from the "back" surface of the specimen, the beam arrives at the detector with its original p-polarization.

An important feature of the interferometer is that, because of the successive front surface/back surface reflections, it is inherently insensitive to translational movements of the specimen which may be caused by the large current pulse during heating. Also, because of lenses L1 and L2, small axial rotations of the specimen do not cause appreciable variations in

optical path difference (PD) between the component beams; a detailed analysis of this effect is given in the Appendix of Ref. 1.

As the specimen is heated, its "length" l changes by an amount Δl, thereby giving rise to a change in optical path difference of

$$\Delta PD = 2\,\Delta l = \lambda\,\Delta n \tag{1}$$

where $\lambda = 632.8$ nm and Δn is the number of fringes that shift through the field of view. An expression for linear thermal expansion of the specimen follows from Eq. (1) as

$$(l - l_0)/l_0 = (\lambda/2l_0)\,\Delta n \tag{2}$$

where l_0 is the reference dimension of the specimen at 293 K.

The light output from the interferometer consists of two superimposed orthogonally polarized beams which cannot interfere to produce fringes unless they are brought to the same polarization plane. This operation is performed by a novel phase-quadrature detector, which is illustrated schematically in Fig. 3. The detector consists of (1) a beam-expanding lens, (2) an interference filter (1-nm passband centered at 632.8 nm) to exclude thermally radiated light from the specimen, (3) a quarter-wave plate with its fast axis at 45°, (4) a four-quadrant analyzer with principal axes as shown, and (5) a four-element silicon photodiode.

The key optical element is the quarter-wave plate, which converts the linear polarizations of the two incoming beams into left- and right-handed circular polarizations, which, in turn, combine into a single linearly polarized beam. Since the polarization orientation ϕ is directly proportional to the phase difference δ between the incoming beams, the maximum

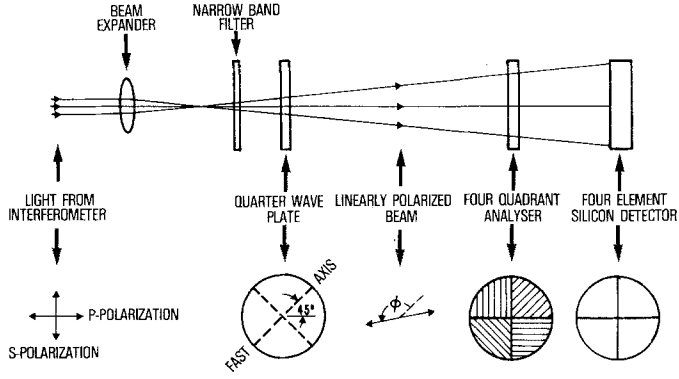

Fig. 3. Schematic diagram of the phase-quadrature detector.

light transmission will rotate through successive quadrants as the specimen expands. It can be shown [1] that, by differentially amplifying the electrical signals from diagonally opposite quadrants, one obtains two signals proportional to $\cos\delta$ and $\sin\delta$, respectively. The signals are in phase quadrature and, therefore, are ideally suited for bidirectional counting of the fringe movements. The cumulative fringe shift Δn may be determined from the change in phase difference via the relation

$$\Delta n = (\delta - \delta_0)/2\pi \tag{3}$$

where δ_0 is the initial phase difference at 293 K.

Figure 4 illustrates the variation of the pyrometer signal and the two

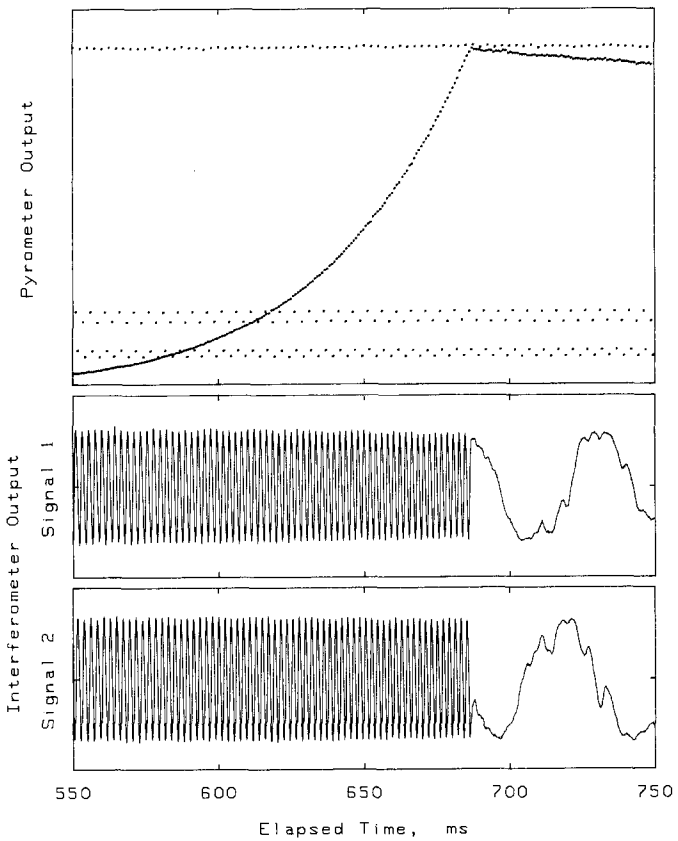

Fig. 4. Variation of the specimen radiance as seen by the pyrometer and the specimen expansion as measured by the interferometer during a typical pulse experiment. Dots forming the horizontal lines in the pyrometer output correspond to radiances from a reference source. Each cycle of the interferometer output corresponds to an expansion of $\lambda/2$.

interferometer signals as a function of elapsed time during a typical pulse experiment. One cycle of either interferometer signal corresponds to a shift of one fringe or a specimen expansion of $\lambda/2$. The two interferometer signals are recorded every 0.1 ms by means of a digital storage oscilloscope (16-kbyte memory, 12-bit resolution). The pyrometer signal is recorded by a second digital oscilloscope, thereby permitting 1200 evaluations of specimen temperature per second.

The initial interferometric system [1] utilized digital oscilloscopes with a smaller memory (4 kbytes) and therefore was limited to recording only one interferometer signal (every 0.2 ms). The background "jitter" associated with the earlier interferometer (about 0.2 fringe) was reduced to less than 0.1 fringe by improved isolation from vibrations, air currents, etc.

4. SUMMARY OF RESULTS

4.1. Refractory Metals

In the earlier measurements, namely, those on tantalum [1] and molybdenum [4], expansion results were based on only one-sixth of the recorded data points corresponding to a single interferometer signal because of limitations in the data acquisition and computational systems. As a result of improvements in these systems and in the method of analysis, the results from subsequent expansion measurements on niobium [5] and tungsten [6] were based on all data recorded for both interferometer signals. In the present paper, all available fringe shift data from the earlier measurements have been reanalyzed to provide a common basis for comparing expansion results for these metals.

The final results for each refractory metal were obtained by using the method of least squares to fit a quartic polynomial in temperature to the expansion/temperature data pairs; the resultant polynomial coefficients are given in Table I. The deviation of individual data pairs from the smooth function for each refractory metal is illustrated in Fig. 5. The scatter among the data pairs (about 0.5% or less) is due primarily to differences between data from different specimens, although uncertainties in determining fringe count from a limited number of data points per fringe ($\sim$20 at 1500 K decreasing to $\sim$10 near the melting point) also contribute.

The smoothed results for linear thermal expansion of niobium, molybdenum, tantalum, and tungsten, as defined by the fitted polynomials, are given at intervals of 100 K in Table II and are illustrated in Fig. 6. Although not readily visible in this graph, correlations among these results exist and may be seen by plotting the dimensionless expansivity $\alpha^* =$

Table I. Results of Fitting, by the Least-Squares Method, Polynomial Functions in Temperature (in K) of the Form $(l-l_0)/l_0 = a_0 + a_1 T + a_2 T^2 + a_3 T^3 + a_4 T^4$ to Expansion/Temperature Data Pairs for Different Metals

Metal	Number of specimens	Temperature range (K)	Number of data pairs	SD[a] (%)	Polynomial coefficient[b]				
					$10^3 a_0$	$10^6 a_1$	$10^9 a_2$	$10^{12} a_3$	$10^{16} a_4$
Niobium	3	1500–2700	1677	0.31	5.4424	−8.8553	12.993	−4.4002	6.3476
Molybdenum[c]	3	1500–2800	1610	0.15	6.4176	−11.919	14.085	−4.8303	7.0820
Tantalum[c]	4	1500–3200	3338	0.20	0.70642	1.1032	4.3824	−1.3720	1.9671
Tungsten	3	1500–3600	2324	0.15	1.3896	−0.82797	4.0557	−1.2164	1.7034
Iron (α)	2	1130–1180	49	0.8	−3.778	14.80	—	—	—
Iron (γ)	3	1200–1330	158	0.8	−18.83	24.37	—	—	—

[a] Standard deviation of an individual value of $(l-l_0)/l_0$ from the smooth function.
[b] Based on the specimen reference length (l_0) at 293 K.
[c] Polynomial coefficients reported earlier [1, 4] were determined by fitting only one of every six expansion/temperature data pairs.

$(1/l_0)\, dl/dT^*$ as a function of dimensionless temperature $T^* = T/T_m$, where T_m is the melting temperature, as shown in Fig. 7; the ratio α^*/T_m is equivalent to $\alpha = (1/l_0)\, dl/dT$, the usual definition of expansivity (or coefficient of thermal expansion). As can be seen, there is a striking similarity in the α^* vs T^* curves for Nb and Ta, which are Group VB metals, and in the curves for Mo and W, which are Group VIB metals.

The measurements on tungsten [6] were performed on specimens fabricated from the Standard Reference Material 737 [9], which is certified by the Office of Standard Reference Materials at NIST as a standard for measurements of thermal expansion at temperatures in the range 80 to 1800 K. As shown in Fig. 8, the expansivity values (SD[3] = $0.11 \times 10^{-6}\,K^{-1}$) derived from our measurements on SRM 737 are in reasonably good agreement (better than $0.15 \times 10^{-6}\,K^{-1}$) with the certificate values [10] (SD = $0.03 \times 10^{-6}\,K^{-1}$) at temperatures common to the two investigations.

[3] Standard deviation of an individual value of expansivity from a smooth function of temperature obtained by the least-squares method.

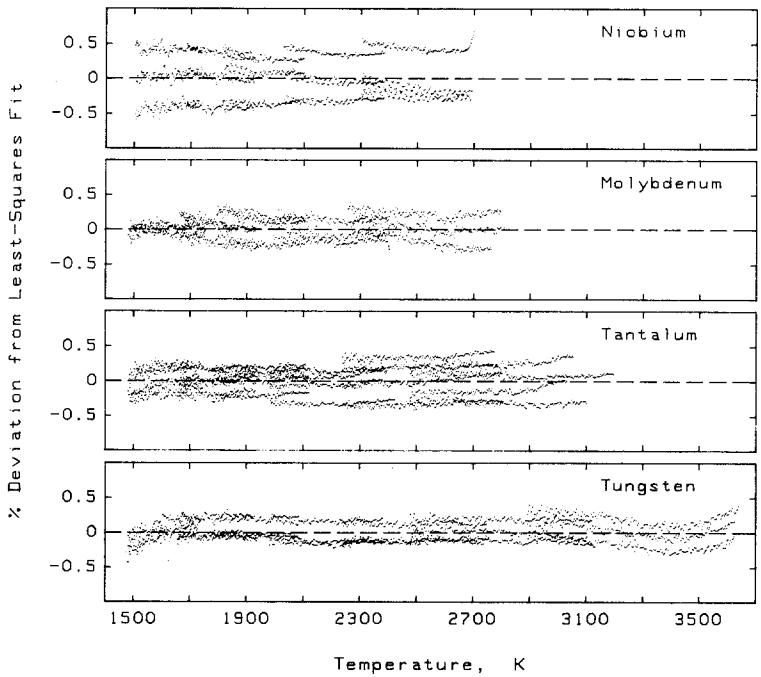

Fig. 5. Deviation of expansion/temperature data pairs from the smooth functions (see Table I) representing the least-squares fits to the data for niobium, molybdenum, tantalum, and tungsten.

4.2. Solid–Solid Phase Transformations

The thermal expansion of iron is of interest because of a particular sequence of solid–solid phase transformations: as temperature is increased, the lattice changes from a body-centered cubic to a face-centered cubic structure ($\alpha \rightarrow \gamma$) at about 1190 K and then, at a somewhat higher temperature (~ 1660 K), returns to the body-centered cubic structure ($\gamma \rightarrow \delta$). In order to establish the applicability of our technique to the study of such transformations, preliminary measurements were performed on iron in the vicinity of its $\alpha \rightarrow \gamma$ transformation [7]. For this work, specimens were fabricated from a polycrystalline rod into long thin rectangular rods with nominal dimensions $2.4 \times 4.2 \times 24$ mm long; the specimen "length" l_0 corresponded to the 4.2-mm dimension.

Table II. Smoothed Results[a] for the Linear Thermal Expansion (%) of Niobium, Molybdenum, Tantalum, and Tungsten

Temperature (K)	$100\,(l-l_0)/l_0$			
	Niobium	Molybdenum[b]	Tantalum[b]	Tungsten
1500	0.976	0.751	0.859	0.603
1600	1.067	0.826	0.936	0.658
1700	1.162	0.904	1.015	0.715
1800	1.260	0.986	1.095	0.773
1900	1.361	1.072	1.178	0.833
2000	1.466	1.161	1.261	0.895
2100	1.574	1.254	1.347	0.958
2200	1.686	1.352	1.434	1.024
2300	1.803	1.456	1.524	1.091
2400	1.926	1.566	1.616	1.160
2500	2.055	1.684	1.710	1.232
2600	2.192	1.811	1.807	1.306
2700	2.338	1.948	1.908	1.383
2800		2.097	2.013	1.464
2900			2.121	1.548
3000			2.235	1.636
3100			2.353	1.729
3200			2.478	1.827
3300				1.931
3400				2.041
3500				2.158
3600				2.283

[a] Based on the specimen reference length (l_0) at 293 K.

[b] Some tabulated values differ by 0.001 from those reported earlier [1, 4] which were determined by fitting only one of every six expansion/temperature data pairs.

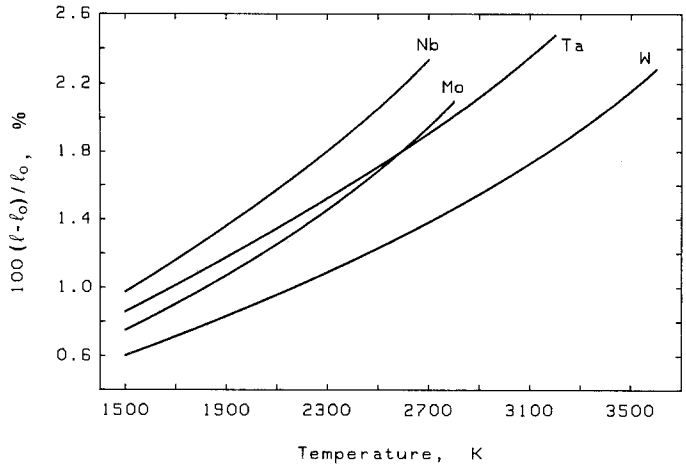

Fig. 6. Smoothed results for the linear thermal expansion of niobium, molybdenum, tantalum, and tungsten as expressed by the polynomial functions given in Table I.

Figure 9 illustrates the variation of one of the interferometer signals as a function of elapsed time during a typical pulse experiment on iron. A reversal in fringe shift is clearly visible at the onset of the $\alpha \rightarrow \gamma$ transformation as the specimen begins to rapidly contract and, again, at the completion of the transformation as the specimen begins to expand again. The change in signal amplitude during the transformation is probably due

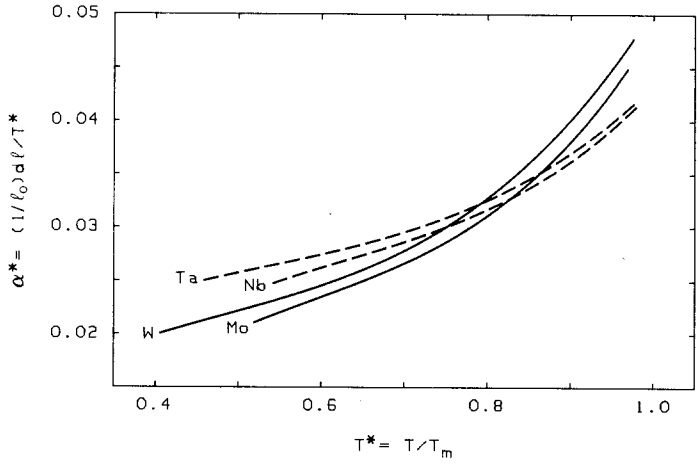

Fig. 7. Dimensionless expansivity α^* as a function of dimensionless temperature T^* for niobium, molybdenum, tantalum, and tungsten.

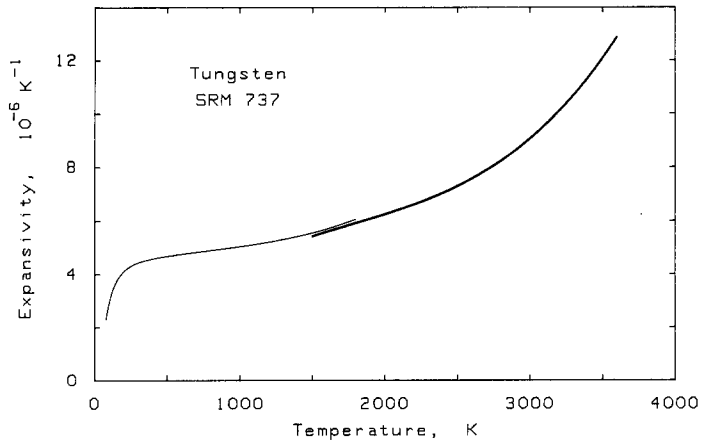

Fig. 8. Expansivity of tungsten SRM 737 as a function of temperature, where the thick solid curve refers to recent data obtained by Miiller and Cezairliyan [6] and the thin solid curve represents the certificate values reported by Kirby and Hahn [10].

to the transitory formation and movement of interphase boundaries at the specimen surface, which, in turn, change the reflectivity of the highly polished flats on opposite sides of the specimen.

The results for thermal expansion of iron in the vicinity of its $\alpha \rightarrow \gamma$ transformation are illustrated in Fig. 10. The scatter in expansion values is primarily the result of random fluctuations in the temperature signal which

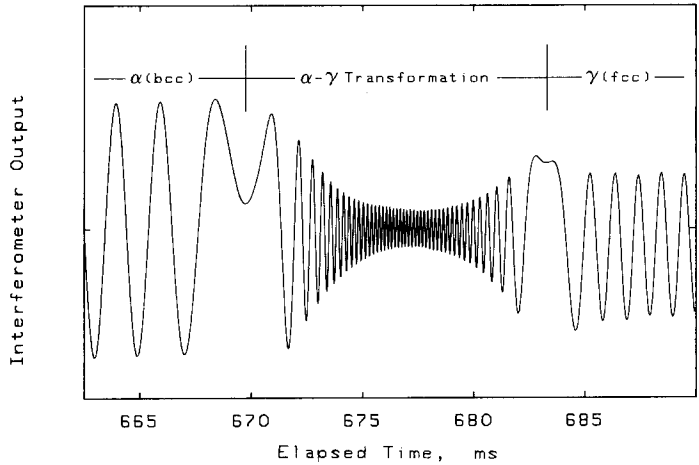

Fig. 9. Variation of the interferometer output as a function of elapsed time during a typical pulse experiment in which iron is rapidly heated through the $\alpha \rightarrow \gamma$ transformation.

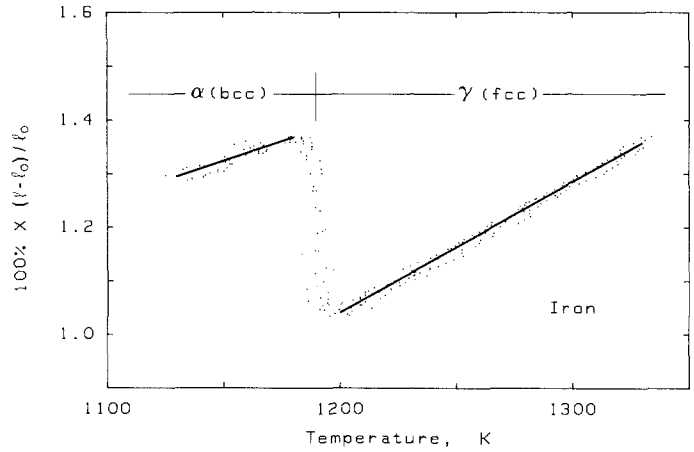

Fig. 10. Linear thermal expansion of iron in the vicinity of the $\alpha \rightarrow \gamma$ transformation. The solid straight lines represent least-squares fits (see Table I) to the data.

arise when the pyrometer is operated well below its optimum temperature range of 1500 K and above. In this work, true temperatures were determined from the measured surface radiance temperatures (at 0.65 μm) by selecting an effective normal spectral emittance that would yield a transformation temperature of 1190 K at the arrest in the measured temperature–time function. The solid straight lines represent linear functions of temperature which were obtained by fitting the data by the least-squares method; the polynomial coefficients are given in Table I. The fractional change in length during the transformation was determined to be 0.366%, which compares favorably with other literature data given in Ref. 7.

4.3. Estimate of Errors

Detailed analyses of errors arising from the measurement of specimen temperature, fringe count, and specimen "length" at 293 K are given in the earlier publications [1, 7]. For the refractory metals, the resultant maximum error in the reported values of linear thermal expansion was estimated to be about 1% at 2000 K, increasing to about 2% at 3600 K. In the measurements on iron, the resultant maximum error, estimated to be about 4%, was due largely to the determination of specimen temperature.

5. CONCLUDING REMARKS

The thermal expansion results obtained for the refractory metals, niobium, molybdenum, tantalum, and tungsten, clearly establish the

applicability of our high-speed interferometric technique to the accurate measurement of thermal expansion at high temperatures, particularly above about 1500 K up to near the melting point of the specimen. A correlation, observed in the α^* vs T^* functions for these refractories (see Fig. 7), appears to be related to the influence of electron band structure on the expansion characteristics of a given metal. It suggests that reasonable estimates of expansivity (to within about 5%) of a given metal may be possible at high temperatures, over a large temperature range, if accurate expansion data for a neighboring metal in the same column of the periodic table are available. Accurate expansion measurements on other Group VB (e.g., vanadium) and/or Group VIB metals (e.g., chromium) would provide additional insights.

As mentioned in Section 4.1, tungsten SRM 737 is certified as a standard for thermal expansion measurements at temperatures between 80 and 1800 K. Our recent measurements [6] on this material should provide a sufficient data base for extending the temperature range of this standard up to 3600 K.

The preliminary study of the $\alpha \rightarrow \gamma$ transformation in iron demonstrates the applicability of our high-speed interferometric technique to following rapid dimensional changes that occur during solid–solid phase transformations. In future experiments on the $\alpha \rightarrow \gamma$ transformation, specimens in the form of precision-machined tubes should be used to minimize the uncertainty arising from the measurement of temperature. Other solid–solid phase transformations, occurring at temperatures within the optimum operating range of the pyrometer, are also possible candidates for further study, such as the $\gamma \rightarrow \delta$ transformation in iron at ~ 1660 K and the $\alpha \rightarrow \beta$ transformation in hafnium at ~ 2000 K, among the pure metals.

REFERENCES

1. A. P. Miiller and A. Cezairliyan, *Int. J. Thermophys.* **3**:259 (1982).
2. A. Cezairliyan, M. S. Morse, H. A. Berman, and C. W. Beckett, *J. Res. Natl. Bur. Stand (U.S.)* **74A**:65 (1970).
3. A. Cezairliyan, *J. Res. Natl. Bur. Stand. (U.S.)* **75C**:7 (1971).
4. A. P. Miiller and A. Cezairliyan, *Int. J. Thermophys.* **6**:695 (1985).
5. A. P. Miiller and A. Cezairliyan, *Int. J. Thermophys.* **9**:195 (1988).
6. A. P. Miiller and A. Cezairliyan, *Int. J. Thermophys.* **11**:619 (1990).
7. A. P. Miiller and A. Cezairliyan, in *Thermal Expansion 8*, T. A. Hahn, ed. (Plenum Press, New York, 1984), p. 245.
8. G. M. Foley, *Rev. Sci. Instrum.* **41**:827 (1970).
9. Office of Standard Reference Materials, *NBS Standard Reference Materials Catalog*, 1988–89 ed., NBS Special Publication 260 (U.S. Government Printing Office, Washington, D.C., 1988).
10. R. K. Kirby and T. A. Hahn, SRM 737 Certificate (Office of Standard Reference Materials, Natl. Bur. Stand. (U.S.), 1976).